



## Rapid and facile microwave-assisted synthesis of $\text{Cu}_2\text{V}_2\text{O}_7$ /graphene nanocomposite as a novel catalyst for degradation of organic dyes

Kaveh Parvanak Boroujeni\*<sup>1</sup>, Zeinab Tohidian\*<sup>2</sup>, Zahra Hamidifar<sup>1</sup> & Mohammad Mehdi Eskandari<sup>3</sup>

<sup>1</sup>Department of Chemistry, Shahrekord University, P.O. Box 88186-34141, Shahrekord, Iran

<sup>2</sup>Department of Chemistry, Shahrekord Branch, Islamic Azad University, Shahrekord, Iran

<sup>3</sup>Nanotechnology Research Center, Research Institute of Petroleum Industry, Tehran, Iran

E-mail: parvanak-ka@sku.ac.ir

Received 25 July 2021; accepted 24 March 2022

For the first time,  $\text{Cu}_2\text{V}_2\text{O}_7$ /graphene nanocomposite with 20–30 nm in size has been prepared by solid state decomposition microwave method in short time. The obtained nanocomposite have been fully characterized by X-ray diffraction (XRD), Fourier-transformed infrared spectroscopy (FT-IR), field emission scanning electron microscopy (FE-SEM), energy-dispersive X-ray spectroscopy (EDX), transmission electron microscopy (TEM), vibrating sample magnetometer (VSM), and UV-Vis spectroscopy. The photocatalytic property of the nanocomposite has been investigated for degradation of methylene blue (MB) and methyl orange (MO) dye pollutants in aqueous solution under solar light (average light intensity of  $180 \text{ mW cm}^{-2}$ ) and ultrasound (250 W) irradiation at room temperature. The band gap of the  $\text{Cu}_2\text{V}_2\text{O}_7$ /graphene nanocomposite is found to be 4.4 eV.

**Keywords:** Dye degradation, Graphene, Magnetic, Microwave irradiation, Nanocomposite, Photocatalysis

Pollution of water bodies poses a threat to the health of humans and other animals. Organic dyes produced by industrial processes are one of the major pollutant factors of water and environment. Nowadays, various treatment techniques such as coagulation, flocculation, reverse osmosis, ultrafiltration, and adsorption have been applied for the removal of dyes<sup>1</sup>. However in these techniques, a secondary waste product can be created which cannot be further destroyed. Photocatalytic degradation reactions are as attractive alternatives, which are able to remove different organic dyes without generation of secondary waste byproducts. The photocatalysis is a green method, in which the oxidation and reduction reactions are performed through photoinduced generation of electron-hole pairs, leading to produce active radical species that cause degradation of dye pollutants<sup>2</sup>. Recently, many research efforts have been focused on the synthesis of different semiconductor-based photocatalysts. Also, the incorporation of graphene as a zero band gap semiconductor into the photocatalyst structure was studied in the context of degradation processes<sup>3</sup>.

Copper vanadates are of interest as inorganic ternary oxides ( $\text{M}_x\text{V}_y\text{O}_z$ ) applicable to photocatalysts,

sensors, quantum magnets, anode materials, water splitting, and so on<sup>4</sup>, due to their unique properties like high gravimetric capacity and energy density. Among these,  $\text{Cu}_2\text{V}_2\text{O}_7$  (pyrovanadate) deserve particular attention. For example,  $\text{Cu}_2\text{V}_2\text{O}_7$  films were prepared via electrostatic spray deposition for use as photoanodes for solar water splitting<sup>5</sup>. Also,  $\text{Cu}_2\text{V}_2\text{O}_7$ /reduced graphene oxide mesoporous microspheres were obtained through hydrothermal method and were used as anode for Lithium battery<sup>6</sup>.  $\text{Cu}_2\text{V}_2\text{O}_7$  nanoparticles prepared by precipitation method have been used as the adsorbent for the removal of the organic dye Congo red<sup>7</sup>. Silicate glass matrix@ $\text{Cu}_2\text{O}/\text{Cu}_2\text{V}_2\text{O}_7$  has been employed for photodegradation of sulfamethoxazole<sup>8</sup>. As far as we know, there is no report for the utilization of  $\text{Cu}_2\text{V}_2\text{O}_7$  or its derivatives as the catalyst for photodegradation of dye pollutants and also in synthetic organic transformations.

So far, the different synthetic methods were reported for the preparation of nanocomposites decorated on graphene including, hydrothermal, co-precipitation, Punica Granatum peel extract, sonochemical method, and so forth<sup>9</sup>. The important factor for choosing synthetic method is cost,

simplicity, safety, meanwhile generation of pure nanoparticles in short time. Recently, we introduced the synthesis of Co–Sn–Cu oxides/graphene nanocomposites using solid-state microwave irradiation method<sup>10</sup>. Along this line, herein we wish to report the synthesis of  $\text{Cu}_2\text{V}_2\text{O}_7$ /graphene nanocomposite by this method from a Schiff base complex precursor. The obtained  $\text{Cu}_2\text{V}_2\text{O}_7$ /graphene nanocomposite was characterized by X-ray diffraction (XRD), Fourier-transformed infrared spectroscopy (FT-IR), field emission scanning electron microscopy (FE-SEM), energy-dispersive X-ray spectroscopy (EDX), transmission electron microscopy (TEM), vibrating sample magnetometer (VSM), and UV-Vis spectroscopy. The photocatalytic activity of  $\text{Cu}_2\text{V}_2\text{O}_7$ /graphene nanocomposite was investigated for the photodegradation of organic dye pollutants under solar and ultrasound irradiation.

## Experimental Section

### Chemicals and apparatus

All the chemical reagents was purchased from Merck, Fluka or Sigma-Aldrich Companies and used in experiments without further purification. Powder X-ray diffraction (PXRD) analysis was recorded on an X-ray diffractometer with Ni-filtered Cu  $K\alpha$  irradiation ( $\lambda = 1.54 \text{ \AA}$ ), for an angle range of  $2\theta = 10\text{--}80^\circ$ . FT-IR 160 spectrophotometer (Shimadzu system) was used for recording FT-IR spectra from 4000 to  $400 \text{ cm}^{-1}$  by KBr tablets.  $^1\text{H}$  NMR spectra were recorded on 400 MHz spectrometer in deuterated chloroform. UV-Vis spectroscopy measurement was obtained by a double-beam Shimadzu 1650 PC at room temperature (298 K). The samples for UV-Vis analysis were well dispersed in 25 mL ethanol, by ultrasonication for 25 min to make a homogeneous suspension. FE-SEM images were taken on a Hitachi s4160/Japan equipped with a link energy dispersive X-ray (EDX) analyzer with gold coating. TEM images were obtained by Philips CM30 at accelerating voltage of 300 kV. The sample was sonicated in EtOH and a drop of the suspension was dried on a carbon-coated micro grid for the TEM analysis. The magnetic property of the sample was measured at room temperature (298 K) using a vibrating sample magnetometer (VSM, MDKFD, Meghnatis Kavir Kashan Co.). Ultrasonic generator was carried out on ultrasonic probe (Top-Sonics UPH-400, ultrasonic technology development Co.). A microwave oven (LG, 2.45 GHz, and 900 W) was

used for the microwave irradiation. Sunny Light measured by CHY 332, Digital Light Meter.

### Synthesis of $\text{H}_2\text{L}$ ligand

The Schiff Base ligand named 4,4'-dibromo-2,2'-[cyclohexane-1,2-diylbis (nitrilomethanylylidene)] diphenol) was prepared according to our previous report.<sup>11</sup> To 10 mL methanolic solution of 5-bromosalicylaldehyde (2 mmol, 0.4 g) was added 10 mL methanolic solution of 1,2-diaminocyclohexane (1 mmol, 0.1 g) and the mixture was refluxed for 1 h. The yellow powder was filtered off, washed with cold methanol, and dried at  $70^\circ\text{C}$ .

### Synthesis of precursor

The precursor was prepared according to our published paper with a little modification.<sup>12</sup> The mixture of  $\text{H}_2\text{L}$  ligand (0.3 mmol, 0.15 g) in methanol (10 mL) was exposed to ultrasonic irradiation. Then, 10 mL of a methanolic solution of  $\text{Cu}(\text{CH}_3\text{COO})_2 \cdot 2\text{H}_2\text{O}$  (0.3 mmol, 0.14 g) and equimolar amount of  $\text{VO}(\text{SO}_4)_2 \cdot 5\text{H}_2\text{O}$  (0.3 mmol, 0.075 g) was added to the above mixture in a drop wise manner. Ultrasonic irradiation (250 W) of the mixture was continued for 15 min at room temperature to form a homogeneous brown solution. After a while, the formed precipitate was separated, washed with cold methanol, and dried under vacuum over anhydrous  $\text{CaCl}_2$ .

### Synthesis of $\text{Cu}_2\text{V}_2\text{O}_7$

First, a porcelain crucible was filled with CuO powder as microwave absorber. Next, 2 g of the precursor powder was added to another porcelain crucible and placed into the first crucible. The assembly was placed in a microwave oven and exposed to microwaves irradiation at 900 W in air for 10 min. Temperature of CuO powder increased from room temperature to  $500^\circ\text{C}$ . After 10 min, decomposition of the precursor was completed. The obtained  $\text{Cu}_2\text{V}_2\text{O}_7$  was cooled to room temperature, washed with water and ethanol, and dried under vacuum over anhydrous  $\text{CaCl}_2$ .

### Synthesis of reduced graphene oxide (rGO)<sup>13</sup>

Phosphoric acid (85%, 10 mL) was placed into a double-jacket reactor and the circulator temperature was adjusted at  $5^\circ\text{C}$ . Concentrated sulfuric acid (90 mL) was added to the mixture and the temperature was set at  $5^\circ\text{C}$  while stirring. Then, a homogeneous solid mixture of graphite (1 g, particle size  $< 50 \mu\text{m}$ ) and potassium permanganate (5 g) was gradually added into the above sulfuric acid-phosphoric acid

solution over a period of 2 h. The mixture was stirred at 5°C and for 3 h. After that, the mixture was stirred with stepwise temperature rise to 25°C for 3 h and then to 55°C in 2 h. Afterwards, the mixture was stirred at 55°C for 12 h, cooled to 5°C, and poured into crushed ice and stirred. Then, by addition of a small volume of hydrogen peroxide (30%) to the resulting mixture an ochre color appeared. After a while, the resulting precipitate was filtered off, washed twice with 50 mL of deionized water and then with concentrated hydrochloric acid (2×10 mL). The washing was repeated with deionized water until sulfate and manganese ions were no longer present in the eluate (checked by barium and sodium bismuthate tests). Finally, the solid product, GO, was washed with ethanol and acetone and dried at 70°C. For preparation of rGO, to a suspension of the obtained GO (500 mg) in water (20 mL), was added 50 mL hydrazine monohydrate. The mixture was refluxed for 24 h at 100°C. The obtained powder, rGO, was washed with water and ethanol and dried under vacuum over anhydrous CaCl<sub>2</sub>.

#### Synthesis of Cu<sub>2</sub>V<sub>2</sub>O<sub>7</sub>/graphene nanocomposite

To 10 mL ethanolic suspension of the rGO (0.1 mg) was added drop wise 10 mL ethanolic suspension of the Cu<sub>2</sub>V<sub>2</sub>O<sub>7</sub> (0.29 mmol, 0.1 g). The mixture was refluxed for 30 min and exposed to ultrasonic irradiation (200 W) for 10 min. The prepared powder was separated by centrifugation, washed with water and ethanol, and dried at 120°C for 12 h.

#### Photocatalytic experimental tests

The photocatalytic activity of the Cu<sub>2</sub>V<sub>2</sub>O<sub>7</sub>/graphene nanocomposite was examined in the removal of organic dyes in aqueous solution under solar and ultrasound irradiation. In the first step, degradation process of dyes was investigated under solar irradiation. The photocatalytic tests were

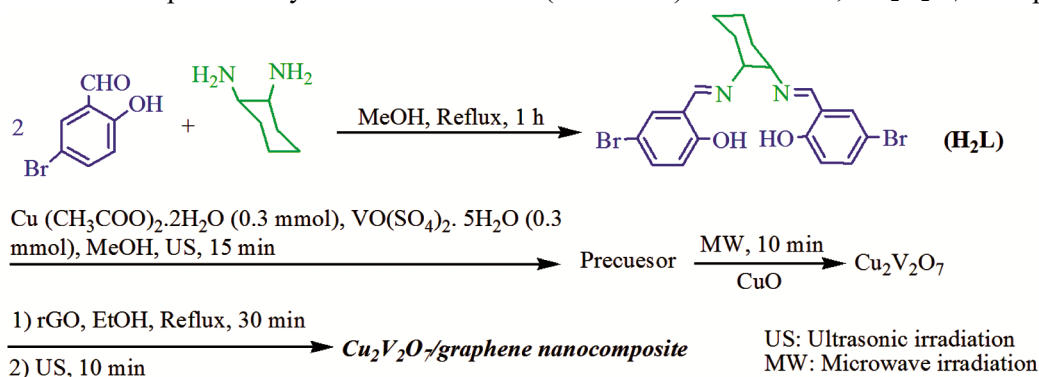
performed on bright sunny days (10 a.m. to 2 p.m., average light intensity of 180 mW cm<sup>-2</sup>) under optimized conditions. Two solutions containing 50 mL of each dye aqueous solution (4 mg/L) were prepared. To the solution of the MB dye 7 mg photocatalyst and 12 mL of H<sub>2</sub>O<sub>2</sub> and to the solution of the MO dye 4 mg photocatalyst and 2 mL of H<sub>2</sub>O<sub>2</sub> were added. The pH of the each solution was adjusted to 7. The mixtures were stirred (500 rpm) at room temperature in the dark for 30 min. In dark condition, adsorption-desorption equilibrium between dye and catalyst was established. Then, the degradation of the dye occurred when the mixture was exposed to solar light. At determined time intervals, the photocatalyst powder was separated by centrifugation (or by an external permanent magnet) of 3 mL of the mixture. After that, degradation process of MB and MO dyes was monitored by measuring the absorptions of MB and MO dyes at 663 and 508 nm, respectively, using a UV-Vis absorption spectrometer. The similar process was performed for degradation of dyes under ultrasound irradiation (250 W) at room temperature. In all experiments, the pH of solution was adjusted to determined values by dropwise addition of NaOH (1 M) or HCl (1 M). The percent of degradation was measured by the following equation:

$$\text{Degradation (\%)} = (C_0 - C_t) / C_0 \times 100$$

where, C<sub>0</sub> is the initial concentration of dye and C<sub>t</sub> is the concentration of dye after the determined time (t).

#### Results and Discussion

For preparation of Cu<sub>2</sub>V<sub>2</sub>O<sub>7</sub>/graphene nanocomposite, firstly a Schiff base ligand (H<sub>2</sub>L) was prepared using 1,2-diaminocyclohexane and 5-bromosalicylaldehyde which then reacted with Cu(CH<sub>3</sub>COO)<sub>2</sub>·2H<sub>2</sub>O and VO(SO<sub>4</sub>)<sub>2</sub>·5H<sub>2</sub>O under ultrasonic irradiation to produce the precursor (Scheme 1). Afterwards, Cu<sub>2</sub>V<sub>2</sub>O<sub>7</sub> was prepared via



Scheme 1 — Synthesis of Cu<sub>2</sub>V<sub>2</sub>O<sub>7</sub>/graphene nanocomposite

solid-state microwave decomposition of precursor in the presence of CuO powder as microwave absorber. In the absence of CuO, the precursor failed to absorb microwaves. During irradiation, the temperature of CuO was raised to 500°C. The generated heat was transferred to precursor, leading to complete decomposition of the precursor. Decomposition of the precursor is accompanied with the evolution of different gases such as N<sub>2</sub>, NO, N<sub>2</sub>O and H<sub>2</sub>O vapours. Finally, Cu<sub>2</sub>V<sub>2</sub>O<sub>7</sub>/graphene nanocomposite was prepared from the reaction of Cu<sub>2</sub>V<sub>2</sub>O<sub>7</sub> with rGO in the presence of ultrasonic irradiation.

Figure 1(a) shows X-ray diffraction (XRD) pattern of Cu<sub>2</sub>V<sub>2</sub>O<sub>7</sub>/graphene nanocomposite. All the diffraction peaks of XRD pattern could be indexed to the Cu<sub>2</sub>V<sub>2</sub>O<sub>7</sub> (monoclinic, space group: C2/c; No. 15, JCPDS Card No. 73-1032) and carbon (hexagonal, space group: P63/mmc; No. 194, JCPDS Card No. 08-0415) phases. The main diffraction peaks were manifested at 2θ = 16.60°, 24.75°, 28.93° and 29.18° which can be perfectly related to (1 1 0), (2 0 0), (1 1 3) and (0 2 2) crystal planes, respectively. Lattice constants of Cu<sub>2</sub>V<sub>2</sub>O<sub>7</sub> phase is calculated as a = 7.687, b = 8.007 and c = 10.090 nm. These observations clearly illustrated Cu<sub>2</sub>V<sub>2</sub>O<sub>7</sub> and graphene phases.

EDX analysis of the Cu<sub>2</sub>V<sub>2</sub>O<sub>7</sub>/graphene nanocomposite was also investigated [Fig. 1(b)]. EDX spectrum of Cu<sub>2</sub>V<sub>2</sub>O<sub>7</sub>/graphene nanocomposite

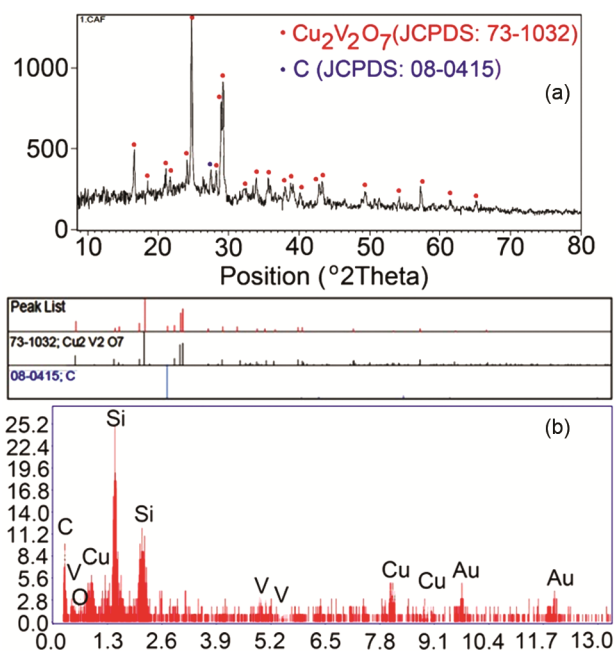


Fig. 1 — XRD pattern of Cu<sub>2</sub>V<sub>2</sub>O<sub>7</sub>/graphene nanocomposite (a) and its EDX spectrum (b)

showed signals of Cu, V, C and, O elements. The observed Si and Au signals were related to metallic coatings of the instrument. EDX analysis proved that the Cu<sub>2</sub>V<sub>2</sub>O<sub>7</sub>/graphene nanocomposite was prepared in high purity by the present synthetic method.

The FT-IR spectra of the precursor and Cu<sub>2</sub>V<sub>2</sub>O<sub>7</sub>/graphene nanocomposite are shown in Fig. 2. In the spectrum of the precursor [Fig. 2(a)], the band at 1609 cm<sup>-1</sup> is related to C=N (azomethine group).<sup>14</sup> In Fig. 2b, a strong band was observed at 700–1000 cm<sup>-1</sup>, which is assigned to the M–O (M= Cu and V) stretching vibrations<sup>15</sup>. The peaks at around 1000 and 1400 cm<sup>-1</sup> are attributed to C–O and C=C of graphene sheet, respectively<sup>16</sup>. The bands appeared at around 2900, 2300, 1380, and 650 cm<sup>-1</sup> are due to the C–H stretching vibration duo to graphene sheets<sup>16</sup>. Also, appearance of broad bands at around 3400 and 1600 cm<sup>-1</sup> were assigned to the stretching and bending vibrations of the water molecules, respectively, absorbed by the sample or KBr. After the microwave irradiation, all characteristic bands of the precursor were disappeared due to complete decomposition of the precursor. Thus, FT-IR data can confirm the structure of Cu<sub>2</sub>V<sub>2</sub>O<sub>7</sub>/graphene nanocomposite.

The morphology of precursor and Cu<sub>2</sub>V<sub>2</sub>O<sub>7</sub>/graphene nanocomposite were surveyed by FE-SEM and TEM analyses. The morphology of precursor is nonrods which were loosely aggregated [Fig. 3(a)]. Figures 3 (b) and (c) show that the morphology of Cu<sub>2</sub>V<sub>2</sub>O<sub>7</sub>/graphene nanocomposite is spherical shape which is confirmed by TEM image [Fig. 3(d)]. Particle size distribution of Cu<sub>2</sub>V<sub>2</sub>O<sub>7</sub>/graphene nanocomposite was estimated to be 20–30 nm

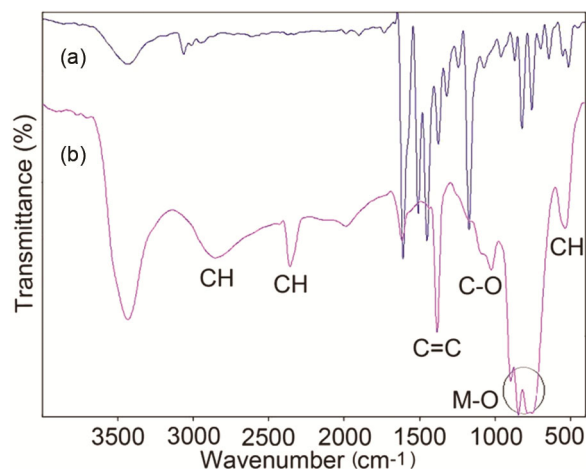


Fig. 2 — FT-IR spectra of the precursor (a) and Cu<sub>2</sub>V<sub>2</sub>O<sub>7</sub>/graphene nanocomposite (b)

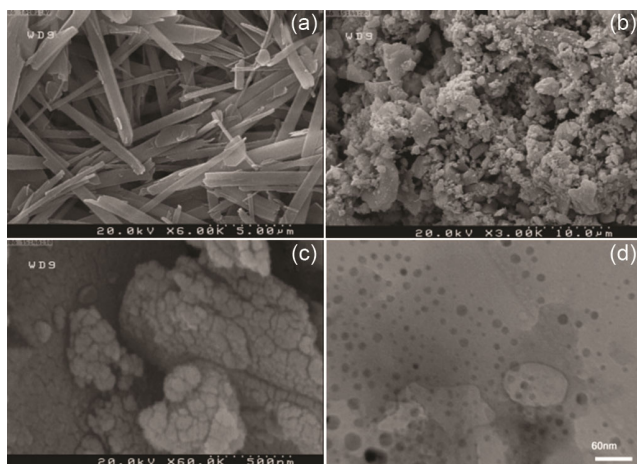


Fig. 3 — FE-SEM images of precursor (a) and Cu<sub>2</sub>V<sub>2</sub>O<sub>7</sub>/graphene nanocomposite (b,c) and TEM image of Cu<sub>2</sub>V<sub>2</sub>O<sub>7</sub>/graphene nanocomposite (d)

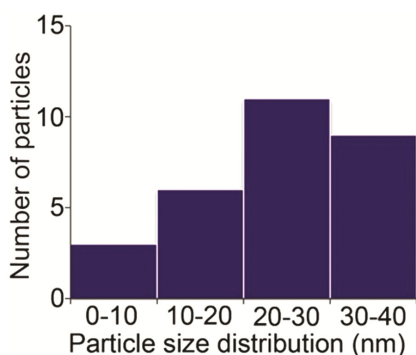


Fig. 4 — Particle size distribution of Cu<sub>2</sub>V<sub>2</sub>O<sub>7</sub>/graphene nanocomposite

(Fig. 4). The morphology of the precursor was not seen in images of Cu<sub>2</sub>V<sub>2</sub>O<sub>7</sub>/graphene nanocomposite, indicating complete decomposition of precursor.

A magnetic property of Cu<sub>2</sub>V<sub>2</sub>O<sub>7</sub>/graphene nanocomposite was investigated using VSM (Fig. 5). The magnetic behaviour of compounds is depended on the type of sample, shape, size, magnetization direction, and synthetic method. The VSM analysis of the Cu<sub>2</sub>V<sub>2</sub>O<sub>7</sub>/graphene nanocomposite shows a weak superparamagnetic behaviour with a remnant magnetization ( $M_r$ ) of 0.9 emu/g.

UV-Vis spectra were recorded for the investigation of electronic property of the synthesized samples. Figure 6(a) shows the UV-Vis spectrum of precursor. The band at 207 nm is related to the  $\pi$ - $\pi^*$  transition of the aromatic rings in ligand structure<sup>17</sup>. The broad band at 470 nm is attributed to the MLCT (metal ligand charge transfer) and LMCT (ligand metal charge transfer) transitions<sup>18</sup>. Figure 6(b) shows

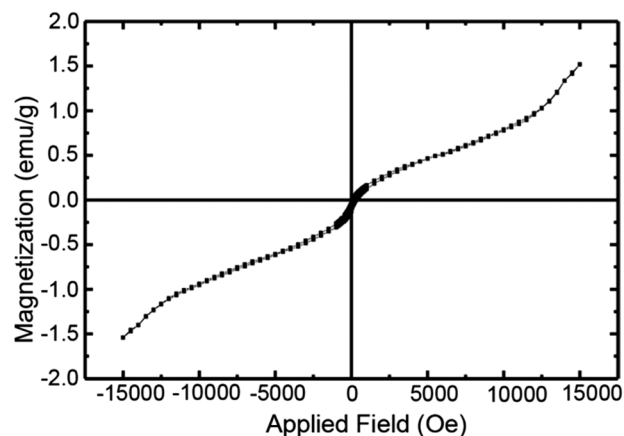


Fig. 5 — VSM analysis of Cu<sub>2</sub>V<sub>2</sub>O<sub>7</sub>/graphene nanocomposite

the electronic spectrum of Cu<sub>2</sub>V<sub>2</sub>O<sub>7</sub>/graphene nanocomposite. The observed bands are due to the electron transitions from 3d orbital of metal (Cu and V) to 2p orbital of oxygen<sup>19</sup>. The band gap ( $E_g$ ) of the synthesized sample can be obtained by the following equation:  $(Ah\nu)^2 = B(h\nu - E_g)$ . In this equation, A,  $h\nu$ , and B are the absorption coefficient, the energy of photon, and a constant related to the type of material, respectively. Fig. 6c shows the  $(Ah\nu)^2$ - $h\nu$  curve for the Cu<sub>2</sub>V<sub>2</sub>O<sub>7</sub>/graphene nanocomposite. The band gap was estimated to be 4.4 eV by extrapolation of the tangent to the X axis. Based on these results, Cu<sub>2</sub>V<sub>2</sub>O<sub>7</sub>/graphene nanocomposite seems to be an attractive candidate in the area of photocatalysis.

The photocatalytic activity of Cu<sub>2</sub>V<sub>2</sub>O<sub>7</sub>/graphene nanocomposite was investigated for degradation of MB and MO organic dye pollutants under solar and ultrasound irradiation. The degradation of MB as a cationic dye was investigated at 663 nm that shows a strong absorption. The characteristic absorption bands of MB dye under the optimized conditions at different times have been shown in Figs. 7 (a) and (b). As Fig. 6a shows the characteristic absorption bands of MB dye is close to zero after 35 min under solar light irradiation, indicating the degradation efficiency of 97 %. Fig. 7(b) manifests the characteristic absorption of MB dye in the presence of ultrasound irradiation. As it can be seen, under ultrasound irradiation the degradation of dye is completed in less time (8 min, efficiency of 96%) than when the solar light was used. During the degradation process, the intensity of the blue colour of the initial solution decreases until it becomes almost colourless, indicating complete degradation of MB dye. Furthermore, the absorption bands of MB dye were not shifted at 663 nm, which

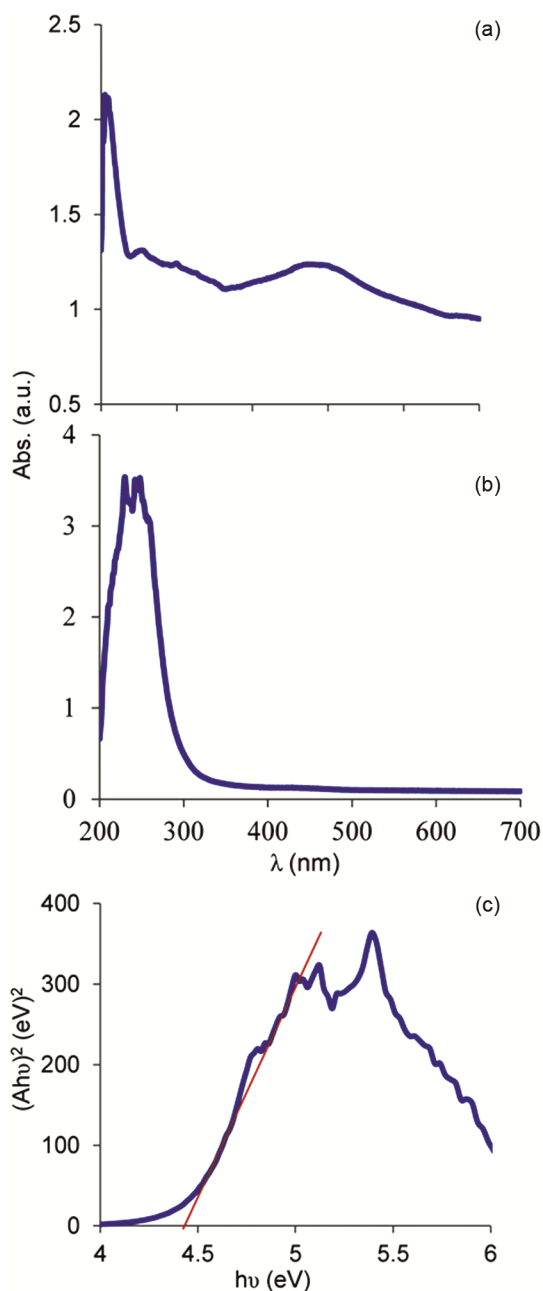


Fig. 6 — (a) Electronic spectra of the precursor; (b) Electronic spectra of  $\text{Cu}_2\text{V}_2\text{O}_7/\text{graphene}$  nanocomposite and (c)  $(Ah\nu)^2-h\nu$  curve of  $\text{Cu}_2\text{V}_2\text{O}_7/\text{graphene}$  nanocomposite

shows that the degradation of MB is due to destruction of chromophore groups.<sup>20</sup> Based on the above results, the  $\text{Cu}_2\text{V}_2\text{O}_7/\text{graphene}$  nanocomposite is an efficacious photocatalyst for the degradation of MB dye both under solar and ultrasound irradiation.

Encouraged by the above results, the photocatalytic activity of the  $\text{Cu}_2\text{V}_2\text{O}_7/\text{graphene}$  nanocomposite was surveyed for degradation of MO dye as a typical anionic dye under similar conditions. The experimental

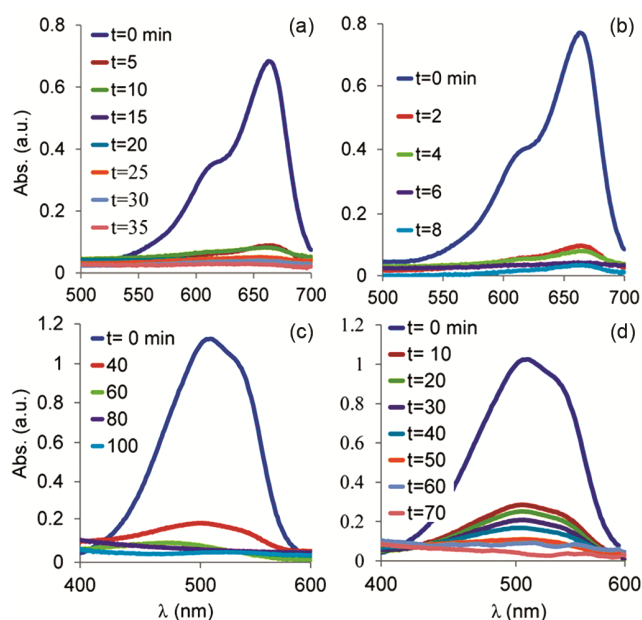


Fig. 7 — Time dependent absorption spectra during degradation process of MB and MO dyes under solar irradiation (a) and (c), respectively, and under ultrasound irradiation (b) and (d), respectively

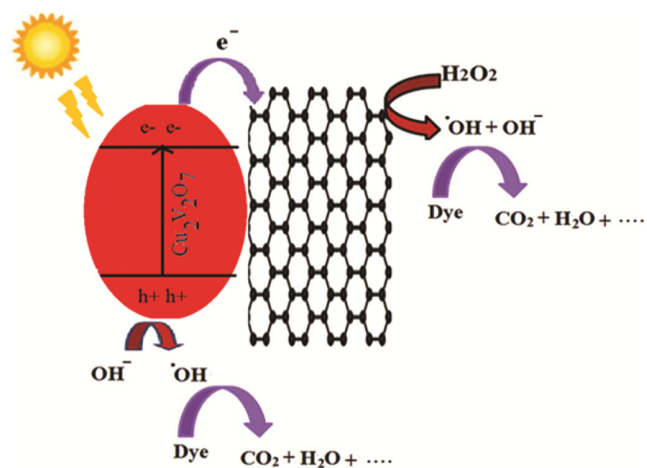
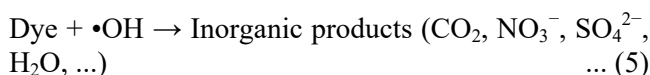
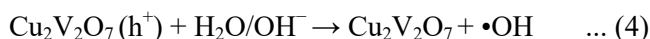
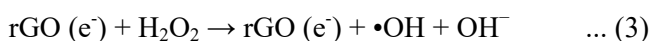
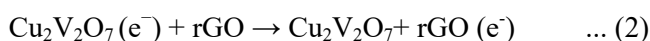
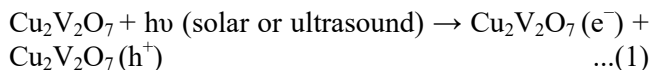


Fig. 8 — A proposed mechanism of degradation of MB or MO dyes over the  $\text{Cu}_2\text{V}_2\text{O}_7/\text{graphene}$  nanocomposite/ $\text{H}_2\text{O}_2$  system at room temperature in aqueous solution

tests were performed under optimized conditions at room temperature. Figures 7(c) and (d) show the changes in intensity of the absorption bands of MO dye as a function of time at 508 nm over of the  $\text{Cu}_2\text{V}_2\text{O}_7/\text{graphene}$  nanocomposite under solar and ultrasound irradiation, respectively. The degradation efficiency for MO was estimated to be 95 % after 100 min under solar irradiation and 97% after 70 min under ultrasound irradiation.

Figure 8 shows the possible mechanism for degradation of MB or MO dyes over

Cu<sub>2</sub>V<sub>2</sub>O<sub>7</sub>/graphene nanocomposite. During irradiation, the appropriate wavelengths could excite Cu<sub>2</sub>V<sub>2</sub>O<sub>7</sub> semiconductor and create electron-hole pairs (Eq. (1)). The generated electrons could transfer easily from the conductive band (CB) of Cu<sub>2</sub>V<sub>2</sub>O<sub>7</sub> to graphene nanosheets to produce rGO (e<sup>-</sup>) (Eq. (2)). It is well known that graphene as a zero bandgap semiconductor has a two-dimensional  $\pi$ -conjugation structure that caused the charge carriers to act as massless fermions<sup>21</sup>. Then, rGO (e<sup>-</sup>) reacted with the H<sub>2</sub>O<sub>2</sub> molecules to afford OH<sup>-</sup> and •OH (Eq. (3)). Also, holes on the valence band (VB) would be reacted with the OH<sup>-</sup> ions and form •OH radicals (Eq. (4)). Finally, the adsorbed dye molecules on the Cu<sub>2</sub>V<sub>2</sub>O<sub>7</sub>/graphene nanocomposite (via the  $\pi$ - $\pi$  stacking or electrostatic attraction), in the presence of the generated •OH radicals were destroyed to some innocent materials, including H<sub>2</sub>O, CO<sub>2</sub>, etc. As it can be seen from Eq. (3), H<sub>2</sub>O<sub>2</sub> leads to the formation of active HO• radicals, resulting in the degradation of dye. However, H<sub>2</sub>O<sub>2</sub> at a concentration more than a critical amount has no effect on the rate of degradation of dye.



The proposed mechanism for degradation of organic dyes under ultrasound irradiation is based on cavitation phenomenon. This phenomenon inclines the formation, growth, and collapse of bubbles in a liquid medium. During the collapse of a cavity, hot spots with high temperature and pressure are generated. Although the lifetime of bubbles is a few microseconds but can generate a relatively wide wavelength range of light (sonoluminescence)<sup>17,21</sup>. The appropriate wavelength of light can excite Cu<sub>2</sub>V<sub>2</sub>O<sub>7</sub> semiconductor and creates electron-hole pairs. Thus, under this condition the concentration of radicals can be raised and consequently the degradation process of dye can proceed in shorter time in comparison to the solar degradation process.

The kinetics of degradation of MB dye over Cu<sub>2</sub>V<sub>2</sub>O<sub>7</sub>/graphene nanocomposite under solar [Fig. 9(a)] and ultrasound irradiation [Fig. 9(b)] were

determined to be the pseudo-second-order model which is represented by the following equation:  $1/C_t = kt + 1/C_0$ , where  $C_0$  and  $C_t$  are the dye concentrations before and after solar or ultrasound irradiation, respectively,  $k$  is the rate constant, and  $t$  is the time of reaction. As shown in Fig. 9, the  $k$  values for the degradation of MB over Cu<sub>2</sub>V<sub>2</sub>O<sub>7</sub>/graphene nanocomposite under solar and ultrasound irradiation were measured to be 0.8365 and 4.0957 min<sup>-1</sup>, respectively. Also, the kinetics of degradation of MO dye over Cu<sub>2</sub>V<sub>2</sub>O<sub>7</sub>/graphene nanocomposite under solar [Fig. 10(a)] and ultrasound irradiation [Fig. 10(b)], were obtained to be the pseudo-first-order model which is represented by the following equation:  $\ln C_t = -kt + \ln C_0$ . The  $k$  values in the presence of solar and ultrasound irradiation were determined to be 0.0318 and 0.0387 min<sup>-1</sup>, respectively. As it can be seen, in the case of MB dye, there is a significant difference between the obtained  $k$  values in the presence of solar and ultrasound irradiation, which may be attributed to degradation mechanism and the kind of dye.

The efficacy of the synthesized Cu<sub>2</sub>V<sub>2</sub>O<sub>7</sub>/graphene nanocomposite for degradation of MB and MO dye pollutants was compared with that of previously reported photocatalysts (Table 1). Obviously, degradation of dyes using Cu<sub>2</sub>V<sub>2</sub>O<sub>7</sub>/graphene

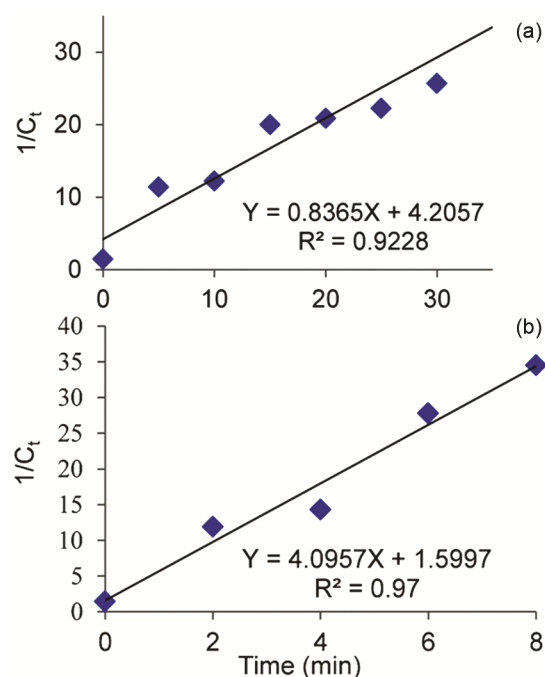


Fig. 9 — Pseudo-second-order kinetic model for degradation of MB dye using Cu<sub>2</sub>V<sub>2</sub>O<sub>7</sub>/graphene nanocomposite under solar (a) and ultrasound irradiation (b)

nanocomposite is superior to many reported procedures<sup>21–27</sup> with respect to reaction time, temperature, degradation efficiency, irradiation source, and the employed synthetic method. In the solid-state microwave decomposition method, used for the preparation of  $\text{Cu}_2\text{V}_2\text{O}_7/\text{graphene}$  nanocomposite, there is an interaction between

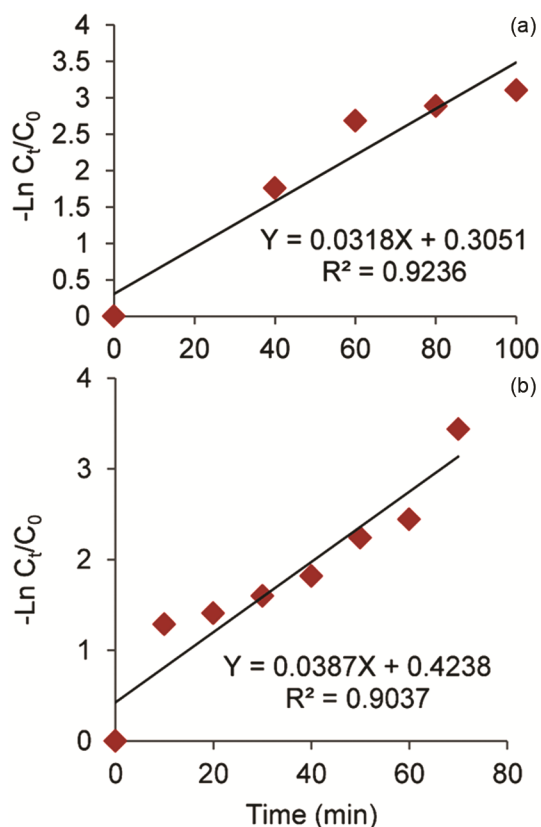


Fig. 10 — Pseudo-first-order kinetic model for degradation of MO dye over  $\text{Cu}_2\text{V}_2\text{O}_7/\text{graphene}$  nanocomposite under solar (a) and ultrasound irradiation (b)

microwave wavelengths and the reactants at the molecular level, resulting in the generation of the electromagnetic energy which is converted to heat by rapid kinetics of the molecules and can improve the chemical reaction.<sup>10</sup>

Stability and recoverability of the catalysts is a main issue in the catalytic tests.  $\text{Cu}_2\text{V}_2\text{O}_7/\text{graphene}$  nanocomposite was separated by an external permanent magnet after each experiment and washed with water and reused for consecutive cycles for degradation of dyes. As shown in Fig. 11,  $\text{Cu}_2\text{V}_2\text{O}_7/\text{graphene}$  nanocomposite did not show significant loss of activity in the degradation of dyes after five repeated cycles. Figure 12 shows FE-SEM images of recoverable  $\text{Cu}_2\text{V}_2\text{O}_7/\text{graphene}$  nanocomposite in photocatalytic degradation of MB dye. It can be seen that the  $\text{Cu}_2\text{V}_2\text{O}_7/\text{graphene}$  nanocomposite do not suffer damage after photocatalytic tests.

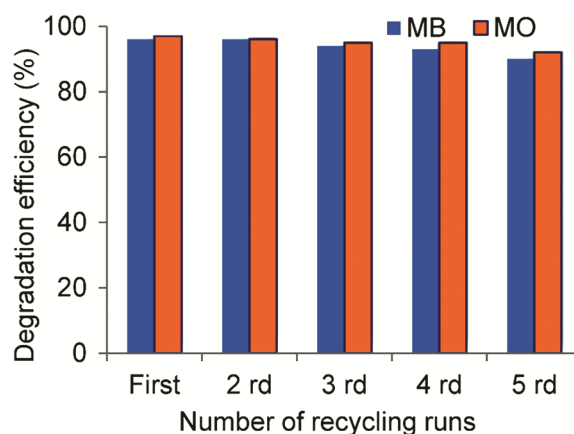


Fig. 11 — Recyclability of  $\text{Cu}_2\text{V}_2\text{O}_7/\text{graphene}$  nanocomposite in photocatalytic degradation of MB and MO dyes in the presence of solar light

Table 1—Comparing the photocatalytic efficiency of  $\text{Cu}_2\text{V}_2\text{O}_7/\text{graphene}$  nanocomposite with some previously reports in degradation of organic dye pollutants

Nanomaterial	Synthetic method	Irradiation	Dye	Degradation efficiency (%)	Time (min)
MIL-101(Cr)/RGO/ZnFe <sub>2</sub> O <sub>4</sub>	Hydrothermal	US <sup>a</sup>	MO	80	70 <sup>21</sup>
CuO	Precipitation	UV	MO	12	120 <sup>22</sup>
CeO <sub>2</sub>	Precipitation	UV	MO	70	120 <sup>22</sup>
Fe <sub>3</sub> O <sub>4</sub> @CuO-RGO	Hydrothermal	UV	MB	94	150 <sup>23</sup>
RGO/ZnO	Ultrasound	UV	MB	87.4	120 <sup>24</sup>
CdS/RGO/carbon nanotube	Hydrothermal	Visible	MB	62	30 <sup>25</sup>
ZnFe <sub>2</sub> O <sub>4</sub>	MW <sup>b</sup> sintering	MW	MB	32	30 <sup>26</sup>
Mn <sub>3</sub> O <sub>4</sub>	Sol-gel	Heating	MB	82	30 <sup>27</sup>
$\text{Cu}_2\text{V}_2\text{O}_7/\text{graphene}$ nanocomposite	MW decomposition	Sunlight	MB	97	35
$\text{Cu}_2\text{V}_2\text{O}_7/\text{graphene}$ nanocomposite	MW decomposition	Sunlight	MO	95	100
$\text{Cu}_2\text{V}_2\text{O}_7/\text{graphene}$ nanocomposite	MW decomposition	US	MB	96	80
$\text{Cu}_2\text{V}_2\text{O}_7/\text{graphene}$ nanocomposite	MW decomposition	US	MO	97	70

<sup>a</sup>Ultrasound

<sup>b</sup>Microwave



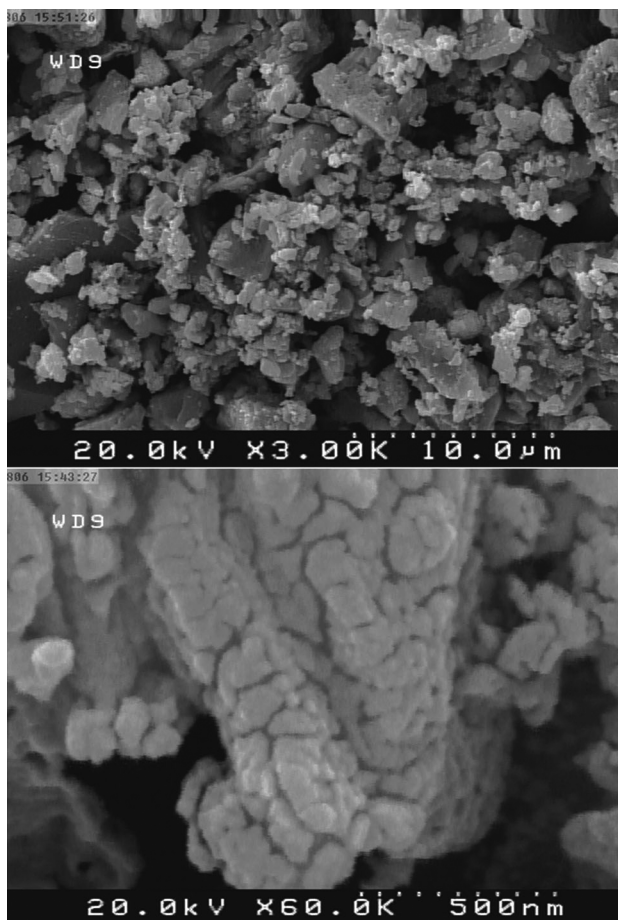


Fig. 12 — FE-SEM images of the recycled Cu<sub>2</sub>V<sub>2</sub>O<sub>7</sub>/graphene nanocomposite after five reaction cycles

### Conclusion

In this study, the Cu<sub>2</sub>V<sub>2</sub>O<sub>7</sub>/graphene nanocomposite has been synthesized by an effective solid state microwave method in short time. The MB and MO were degraded over Cu<sub>2</sub>V<sub>2</sub>O<sub>7</sub>/graphene nanocomposite with high efficiency under solar and ultrasound irradiation. The results showed that degradation times of dyes were decreased in the presence of ultrasound irradiation, duo to sonodegradation process.

### Acknowledgements

The authors gratefully acknowledge Shahrekord University, Shahrekord Branch Islamic Azad University, and Research Institute of Petroleum Industry for their financial support.

### References

- Molla A, Li Y, Mandal B, Gu S, Seung K, Hur H & Suk Chung J, *Appl Surf Sci*, 464 (2019) 170.
- Kumar A & Pandey G, *Mater Sci Eng Int J*, 1 (2017) 1.
- Mandal S K, Dutt K, Pal S, Mandal S, Naskar A, Pal P K, Bhattacharya T S, Singha A, Saikh R, De S & Jana D, *Mater Chem Phys*, 223 (2019) 456.
- Seabold J A & Neale N R, *Chem Mater*, 27 (2015) 1005.
- Kim M, Joshi B, Yoon H, Ohm T Y, Kim K, Al-Deyab S S & Yoon S S, *J Alloys Compd*, 708 (2017) 444.
- Wang Y, Cao L, Huang J, Lu J, Zhang B, Hai G & Jia N, *J Alloys Compd*, 724 (2017) 421.
- Rao M P, Akhila A K, Wu J J, Asiri A M & Anandan S, *Solid State Sci*, 92 (2019) 13.
- Kumar A, Kumar Sharma S, Sharma G, Guo C, Vo D V N, Iqbal J, Naushad Mu & Stadler F J, *J Hazard Mater*, 402 (2021) 123790.
- Hafeez H Y, Lakhera S K, Ashokkumar M & Neppolian B, *Ultrason Sonochem*, 53 (2019) 1.
- Parvanak Boroujeni K, Tohidian Z, Lorigooini Z, Hamidifar Z & Eskandari M M, *IET Nanobiotechnol*, 15 (2021) 197.
- Ebrahimipour S Y, Sheikhshoae I, Castro J, Dúsek M, Tohidian Z, Eigner V & Khaleghi M, *RSC Adv*, 5 (2015) 95104.
- Tohidian Z, Sheikhshoae I, Khaleghi M & Mague J T, *J Mol Struct*, 1134 (2017) 706.
- Parvanak Boroujeni K, Tohidian Z, Fadavi A, Eskandari M M & Shahsanaei H A, *Chem Select*, 4 (2019) 7734.
- Sheikhshoae I, Tohidian Z & Khaleghi M, *Int J Nano Dimens*, 7 (2016) 127.
- Abazari R & Mahjoub A R, *Ind Eng Chem Res*, 56 (2017) 623.
- Ding J, Liu L, Xue J, Zhou Z, He G & Chen H, *J Alloys Compd*, 688 (2016) 649.
- Tohidian Z & Sheikhshoae I, *Rend Fis Acc Lincei*, 28 (2017) 405.
- Lotfi N, Sheikhshoae I, Ebrahimipour S Y & Krautscheid H, *J Mol Struct*, 1149 (2017) 432.
- Gupta D, Meher S R, Illyaskutty N & Alex Z C, *J Alloys Compd*, 743 (2018) 737.
- Xia S, Zhang L, Pan G, Qian P & Ni Zh, *Phys Chem*, 17 (2015) 5345.
- Nirumand L, Farhadi S, Zabardasti A & Khataee A, *Ultrason Sonochem*, 42 (2018) 647.
- Gnanasekaran L, Hemamalini R, Saravanan R, Ravichandran K, Gracia F, Agarwal S & Gupta V K, *J Photochem Photobiol B*, 173 (2017) 43.
- Ding J, Liu L, Xue J, Zhou Z, He G & Chen H, *J Alloys Compd*, 688 (2016) 649.
- Peng Y G, Ji J L & Chen D J, *Appl Surf Sci*, 356 (2015) 762.
- Wang C, Cao M, Wang P & Ao Y, *Mater Lett*, 108 (2013) 336.
- Dom R, Subasri R, Radha K & Borse P H, *Solid State Commun*, 151 (2011) 470.
- Sheikhshoae I, Ramezanpour S & Khatamian M, *J Mol Liq*, 238 (2017) 248.